Negative ion resonances of O_2 adsorbed on Ag surfaces

2000 J. Phys.: Condens. Matter 12 R53

(http://iopscience.iop.org/0953-8984/12/6/201)

J. Phys.: Condens. Matter **12** (2000) R53–R82. Printed in the UK PII: S0953-8984(00)06108-7

REVIEW ARTICLE

Negative ion resonances of O_2 adsorbed on Ag surfaces

R Franchy†+, F Bartolucci†, F Buatier de Mongeot‡, F Cemic‡, M Rocca‡, U Valbusa‡, L Vattuone‡, S Lacombe§, K Jacobi§, K B K Tang‖*, R E Palmer‖, J Villette¶, D Teillet-Billy¶ and J P Gauyacq¶

† Institut für Grenzflächenforschung und Vakuumphysik des Forschungszentrums Jülich, D-52425 Jülich, Germany

‡ Centro di Fisica delle Superfici e delle Basse Temperature del CNR and Istituto Nazionale per la Fisica della Materia, Dipartimento di Fisica, via Dodecaneso 33, 16146 Genova, Italy

§ Fritz-Haber-Institut der Max-Planck-Gesellschaft, D-14195 Berlin, Germany

‖ Nanoscale Physics Research Laboratory, School of Physics and Astronomy, The University of Birmingham, Edgbaston, Birmingham B15 2TT, UK

¶ Laboratoire des Collisions Atomiques et Moléculaires (Unité associée au CNRS 281), Université Paris-Sud, Bâtiment 351, 91405 Orsay, France

E-mail: r.franchy@fz-juelich.de

Received 16 July 1999, in final form 26 October 1999

Abstract. This article gathers together a collection of recent experimental studies of the adsorption of oxygen on (001), (110) and (111) crystal surfaces of silver with special emphasis on the negative ion states of this model system for oxygen adsorption. These investigations were performed in a network entitled 'Negative ion resonances of adsorbed molecules' supported financially by the European Union within the 'Human capital and mobility programme'. The kinetics and thermodynamics of adsorption are investigated by measuring the sticking coefficient and by thermal desorption spectroscopy (TDS). The vibrational spectra provided by high-resolution electron energy loss spectroscopy (HREELS) are used to analyse the adsorbed species (physisorbed and chemisorbed) in the case of O_2 on Ag(110) and on Ag(111). The mechanisms of inelastic electron scattering by adsorbed O_2 are further investigated with special reference to the negative ion resonances (NIRs), formed by electron capture, which are involved in the electron–molecule collision process.

1. Introduction

The O_2–Ag system has recently developed into a model system for the understanding of the interaction of a gas-phase molecule with a solid surface. The reasons for this development arise from the fact that oxygen chemisorption, in particular, and oxidation reactions in general, are of paramount importance for both fundamental and applied studies [1]. The O_2–Ag system looks simple enough to provide hope that we can reach a complete description of the adsorption reaction, yet it is complex enough to allow us to draw general conclusions. Moreover, this system is particularly intriguing because of the central, and so far not entirely explained, role played by adsorbed oxygen in the partial oxidation reaction of ethylene to ethylene epoxide [2] for which Ag substrates show a special selectivity. A large number of good papers on this subject have been published over the last decade dealing in particular with O_2 and O on

+ Corresponding author.

* Current address: Edwards High Vacuum International, Manor Royal, Crawley, West Sussex RH10 2LW, UK.

Ag(110) (see e.g. [3–24]). The other low-Miller-index surfaces have attracted somewhat less attention because of their lower reactivity (see [4, 25–27] for O_2–Ag(111) and [28–32] for O_2–Ag(001)). Taken together these investigations showed (i) that the dissociative adsorption of dioxygen on Ag is activated and proceeds via a negatively charged chemisorbed precursor of peroxo type; this is characterized by a total charge transfer of approximately one electron to the molecule [33], and an internal vibrational frequency of 80 meV, strongly down shifted compared to the gas-phase value of 194 meV, (ii) that three wells are present, corresponding to physisorption, chemisorption and dissociative chemisorption, and (iii) that the adsorption process is strongly anisotropic with respect to the crystallographic face, with the sticking coefficient on the (110) face being about three orders of magnitude larger than on the (111) face.

In the present report we will demonstrate that the reality of this prototype system is even richer. The chemisorbed O_2^- state was accessed either by overcoming the adsorption barrier with the help of a supersonic molecular beam, which allows one to select the impact energy and angle of incidence [18–22, 30, 32, 34, 35], as done in Genova, or by first trapping the molecule in the physisorption well with the crystal cooled with liquid He, and than exploiting the conversion into the chemisorbed state which takes place when heating the crystal, as done in Berlin [36], Birmingham [16] and Jülich [37, 38]. Two vibrational modes (at 79.5 meV and 85 meV) were observed by high-resolution electron energy loss spectroscopy (HREELS) in the molecularly chemisorbed regime both for Ag(001) [39] and Ag(110) [37, 38]. For Ag(110) one of these species desorbs at $\sim$100 K and therefore escaped previous investigations. Only this state can be accessed by conversion from the physisorption well for Ag(110). For Ag(001), in contrast, both moieties are stable up to 150 K.

A description of negative ion resonance scattering (NIR) by molecules adsorbed on surfaces can be found in the reviews of Sanche [40] and Palmer and Rous [41]; resonance scattering in the gas phase has been a well established phenomenon since the 1960s [42]. Andersson and Davenport in 1978 [43] found the first evidence for the formation of NIR at surfaces, for the system OH/NiO(111). Resonance scattering was then observed for several physisorbed molecules [40, 41, 44, 45]. In an increasing number of chemisorption studies (e.g. C_6H_6/Pd(100) [46] and HCOO/Ni(110) [47]) resonance scattering has been observed. Resonance scattering leads to a set of typical properties and in particular to an energetically selective enhancement of a specific vibrational mode together with, typically, the observation of intense overtones of this mode [48]. One of the aims of the present paper is to explore and exploit the specificities of resonant electron scattering for the widely unexplored oxygen on Ag system.

This paper is organized as follows: section 2 deals with the initial sticking coefficient of oxygen on Ag(001) and Ag(110). In section 3, the observation of NIR behaviour in O_2 physisorbed on Ag(111) is demonstrated. Section 4.1 describes experimental studies of NIR scattered by physisorbed O_2 on Ag(110) while section 4.2 presents experimental and theoretical investigations of the angular distribution of NIR of O_2 on Ag(110). Section 5 deals with the nature of the chemisorbed and physisorbed states of O_2 on Ag(110). The paper ends with a summary of what we have learnt about the O_2/Ag system from these resonance studies.

2. Dynamics of the molecule surface interaction and initial sticking coefficient of O_2 on Ag(100) and Ag(110)

The investigation of the dynamics of the O_2–Ag gas–surface interaction via deposition of the O_2 by a supersonic molecular beam allows the angle and the energy of the incident molecules

to be controlled easily. The impact energy of the molecules can be varied either by heating the nozzle (a procedure which affects both translational energy and internal degrees of freedom of the molecules) and/or by seeding the O_2 molecules in He (which affects only the translational motion). Collisions during the supersonic expansion of the gas mixture cause equilibration of its velocity components [49]. Using typically 3% concentrations of the heavier component, impact energies (E_i) of up to 1.1 eV can be reached for O_2. Beam energy and flux were determined by time of flight with a quadrupole mass spectrometer and by a spinning rotor gauge, respectively [50]. The sticking coefficient can be measured either directly by the retarded reflector method developed by King and Wells [51] (henceforth KW) or indirectly by monitoring the variation of coverage with exposure. The former method is very accurate when the sticking coefficient is larger than a few percent and allows an accurate determination of the surface coverage, $\Theta(O_2)$, from the integral of missing O_2 pressure over exposure time. For very low sticking coefficients either thermal desorption spectroscopy (TDS) or high-resolution electron energy loss spectroscopy (HREELS) were used to monitor the coverage. Details of the experimental apparatus in Genova and the surface preparation can be found elsewhere [21, 50].

The energy and angle dependence of the initial sticking coefficient S_0 is shown in figure 1 for Ag(001). In (a) we report data deduced from the coverage–exposure curves estimated by the intensity of the HREELS loss associated with the dipole active intermolecular stretch vibration. Similar curves were measured for O_2–Ag(110) [19, 21] and were confirmed by an independent investigation in Amsterdam [52]. As one can see the data scale with normal energy, $E_n = E_i \cos^2 \theta_i$, as indeed expected for a flat surface for which only the vertical component of the velocity needs either to be dissipated at the first strike in order to allow to reach the trapped state or plays a role in overcoming a potential energy barrier. S_0 grows by three orders of magnitude between $E_n = 20$ meV and $E_n = 0.8$ eV indicating that the process is activated. No enhancement at low impact energy is present although under such conditions trapping in the physisorption well is expected to become important. An increase of S_0 was observed for most systems when lowering E_i below the energy corresponding to the physisorption well depth (approximately 100 meV) [53, 54]. Such an effect is absent, to our knowledge, only for O_2–Ag and N_2–Fe(111) [55]. Both systems are characterized by activated non-dissociative chemisorption but no clear understanding exists so far for the different behaviour of e.g. O_2 on Pt, where trapping has a strong influence on $S_0(E_n)$. Moreover physisorbed O_2 is known to convert to chemisorbed O_2^- (peroxide) at higher coverage of the physisorbed species for Ag(110). For the latter conditions a molecular dynamics study showed that the axis of the molecules lies nearly parallel to the surface pointing along ⟨100⟩, while for dilute conditions the ⟨110⟩ direction is preferred ([38] and see below section 4).

In part (b) of figure 1 we report sticking coefficient data recorded with the more accurate, but less sensitive, KW method. S_0 has a maximum at 0.6 eV and decreases slowly thereafter. A similar behaviour was also reported for Ag(110) by Kleyn *et al* [52], for which, however the behaviour at higher energies is less pronounced (Vattuone *et al* [51]). Such an effect is indicative of the ability of energetic molecules to overcome the chemisorption barrier again after the collision with the Ag atoms of the surface. The difference from Ag(110) is associated with the different corrugation of the chemisorption potential, which is also responsible for the deviation from normal energy scaling.

The KW sticking data recorded at $E_i = 0.39$ eV and 0.8 eV for the 'open' (001) and (110) Ag surfaces are compared in figure 2. By inspection one can see that the data in (a) and (b) corresponding to Ag(001) and the close-packed direction of Ag(110) coincide within experimental error. In both cases we observe overall scaling with E_n although the points at

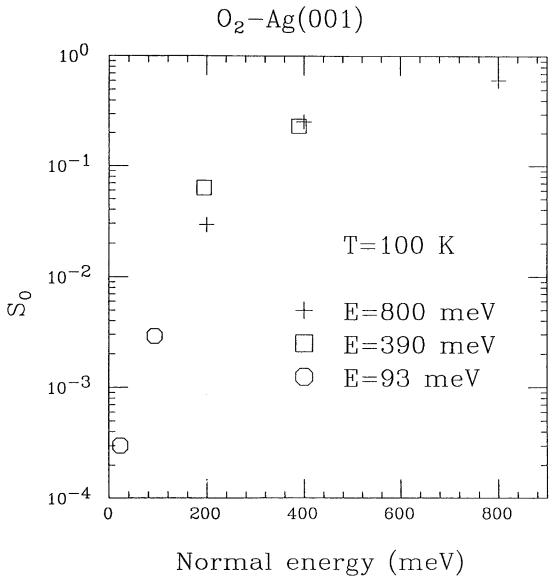

(a)

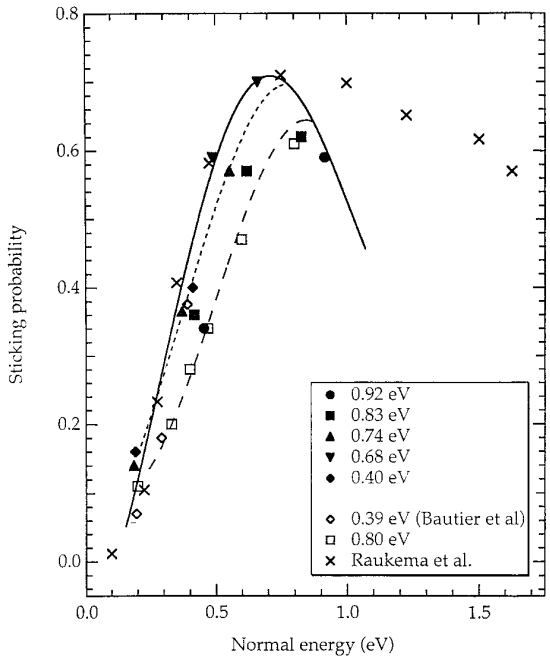

(b)

Figure 1. Dependence of the non-dissociative sticking coefficient on E_n for Ag(001): (a) for coverage–exposure data (from [34]); (b) KW measurements (from [51]). The dotted line in (b) indicates the behaviour reported for Ag(110) [52].

$E_i = 390$ meV and normal incidence are clearly higher than the points recorded at the same E_n but for $E_i = 800$ meV, because of the inelastic interaction with the corrugated chemisorption

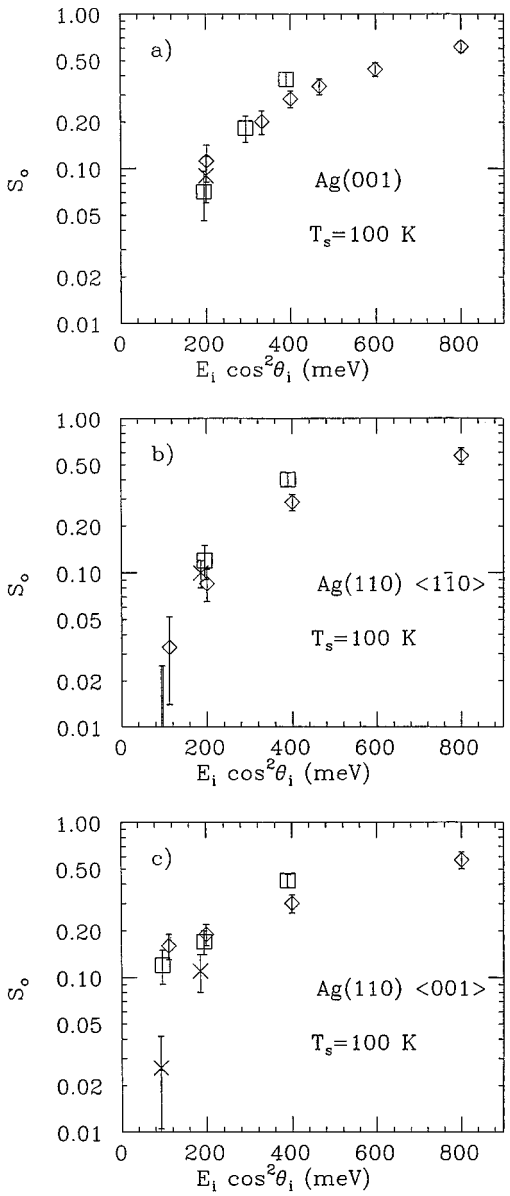

Figure 2. Retarded reflector measurements of the sticking coefficient of O_2 on (a) Ag(001), (b) Ag(110)⟨110⟩, (c) Ag(110)⟨001⟩ against E_n. As one can see the data coincide for the flat Ag(001) surface and for the flat ⟨110⟩ direction of the one-dimensionally corrugated Ag(110) surface (from [35]).

potential. The data recorded for Ag(110) along ⟨001⟩, see figure 2(c), show the same behaviour at large E_i but the spread can be eliminated assuming a dependence with $E_{eff} = E_i \cos^n \theta_i$ with $n \approx 1$ indicating that parallel momentum also helps in overcoming the barrier. As demonstrated theoretically by Darling and Holloway [56] a corrugation can produce this effect by a steering action on the impinging molecules. The physical picture behind this is that the translational energy is most effective in overcoming the barrier when the molecules impinge

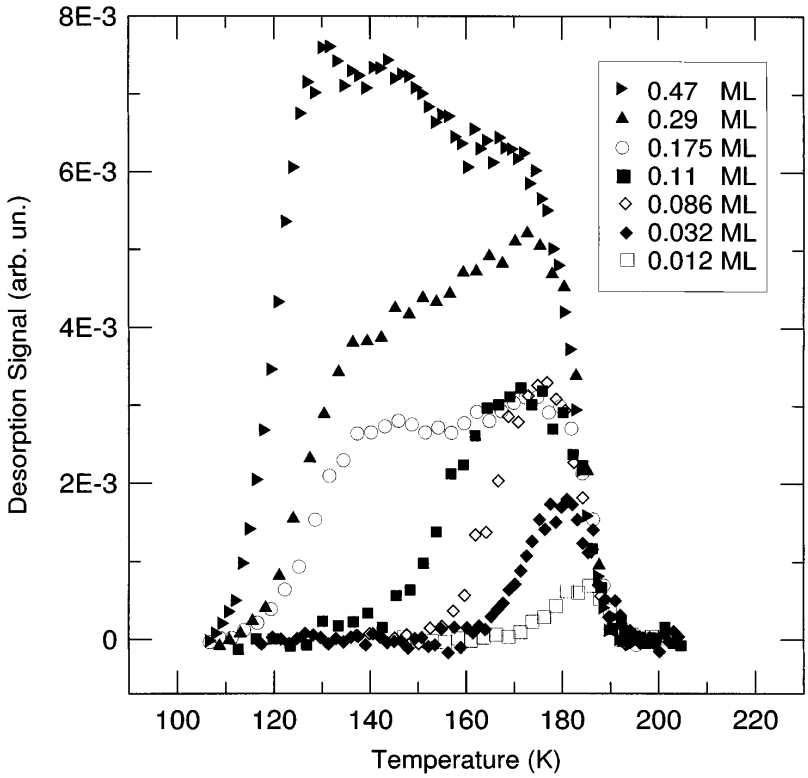

Figure 3. Thermal desorption spectra from O_2 on Ag(001) against O_2 coverage. As one can see a strong shoulder develops on the low-temperature side. Contrary to expectation, the signal at 160 K however continues to grow (from [57]).

along the local normal to the surface. Such an effect dominates at low impact energy where the steering is most effective.

To be more quantitative the dependence of S_0 on impact energy and angle is generally described by the functional form:

$$S_0(E_{eff}) = \eta \int_0^{E_{eff}} \exp -(E_{eff} - E_0)^2 / W^2 \, \mathrm{d}E_{eff}$$

which allows us to estimate the average height of the distribution of barriers to adsorption, E_0, and its width, W. E_0 and W turn out to be 368 ± 50 meV and 167 ± 25 meV, respectively, identical within experimental error for all surfaces and directions.

The average barrier found in the present experiment is thus much higher than the value determined by TDS [4]. Such a finding is connected with the fact that with the beam we are averaging over the whole unit cell and over all possible orientations of the impinging molecules. In contrast, in a TDS experiment the adsorbed molecules have time to search for the lowest energy path which allows them to leave the surface.

The sticking probability, S, is strongly influenced by surface coverage due to the charged state of the admolecules. In the limit of high coverage an exponential decrease of S was observed for Ag(001). In TDS a growth of a strong shoulder at lower temperatures is observed with coverage. The thermal desorption spectra thereby show the particularity that the higher temperature peak does not saturate (see figure 3) [58]. Such behaviour

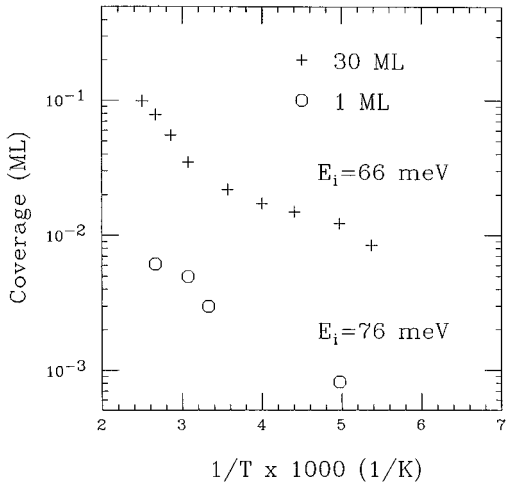

Figure 4. Atomic oxygen coverage obtained by thermal dissociation of O_2 at two different coverages on Ag(001) [34].

could be qualitatively reproduced by de Mongeot *et al* [58] who demonstrated that this feature is strictly determined by the exponential $S(\Theta) = S_0\,e^{-(20\Theta)}$ dependence, whereby the constant is a measure of the repulsive interaction between the admolecules. The anharmonicity of the molecular potential was also analysed against $\Theta(O_2)$ [59]. Both overtones and combined modes were observed indicating a strong, coverage dependent anharmonicity. In particular the frequency shift of the internal stretch vibration of the O_2 molecule with $\Theta(O_2)$ is smaller than expected, due to dipole–dipole interaction, indicating that it must be counterbalanced by a strong chemical shift towards lower frequencies. Both the intermolecular bond and the bond to the surface are thus weakened by an increase in surface coverage.

At room temperature very similar initial sticking–energy curves were measured as seen in figure 1(a), except that the absolute values of S_0 are multiplied by the dissociation probability P_{diss}. This result and the non-observation of loss peaks corresponding to O-adatom vibrations after adsorption at low crystal temperature prove that dissociative adsorption is always promoted by molecular adsorption and takes place eventually only if the crystal temperature is high enough. Collision induced dissociation can be observed for E_i above 0.8 eV. At low coverage P_{diss} turned out to be 0.63 on Ag(110) and 4.4×10^{-3} on Ag(001). The value for Ag(110) decreases with crystal temperature, T, as expected due to competition between desorption and dissociation; in contrast for Ag(001) it increases with T as shown in figure 4. Such anomalous dependence indicates that dissociation on Ag(001) is induced by thermally activated defects [34]; on Ag(110) it also takes place on the atomically flat terraces. Indeed it was recently proven by STM that for Ag(110) at room temperature the supply of Ag adatoms necessary to form the Ag–O adrows of the $(n \times 1)$ reconstructions is not rate limiting for the dissociation reaction [23]. The oxygen molecules can therefore dissociate and can search eventually for the Ag adatoms necessary to form the adrows. In contrast on Ag(001) most of the O_2 admolecules on the terraces desorb.

The O_2–Ag potential energy surface was also investigated in Genova by collision with Xe and Ar atoms at hyperthermal energies for Ag(110) [60] and Ag(001) [61] covered with peroxide. Interestingly, in the collision induced processes the dissociation probability for O_2

on Ag(001) and Ag(110) are nearly equal. The strong anisotropy between the two faces is thus removed when the energy for dissociation is transferred in a local process.

Finally for O_2–Ag(111) at an ambient gas temperature, in contrast with earlier findings [46, 57], we found that the non-dissociative adsorption $S_{M,O}$ is very small ($S_{M,O} < 1 \times 10^{-8}$) [62] which is near to the value of Buatier de Mongeot *et al* [27] who estimated $S_{M,O} < 6 \times 10^{-7}$ [62]. Our upper limit of 1×10^{-8} is smaller by a factor of 50 than the value derived from the data of Raukema *et al* [46] which may be attributed to a smaller number of surface imperfections in our case [62]. The probability for the transiently trapped molecules (reported by Raukema and Kleyn [26]) to evolve into the chemisorbed state depends therefore on the presence of defects or coadsorbates. According to the result of Butler *et al* [63], only molecules with a kinetic energy larger than 0.2 eV can overcome the activation barrier for molecular chemisorption.

3. Physisorption of O_2 on Ag(111)

The Ag(111) surface is thus suitable to study physisorption of molecular dioxygen. By lowering the surface temperature to 20 K, one is able to condense physisorbed mono- or multilayers of O_2 with a high sticking coefficient (near to unity) as known for many physisorption systems. The measured HREEL spectra are easy to interpret since there is no coadsorption of chemisorbed O_2 as found for the other low-index surfaces of Ag (see the following sections).

Figure 5 shows HREEL spectra for an O_2 dose of 1 L [36]. From the change of this spectrum for higher doses (see also figure 9 below) it can be concluded that the coverage is about one monolayer. The energy resolution is 3 meV, an unprecedentedly low value for an He cooled surface. Besides the O–O stretching mode at 0.192 eV its first (at 0.382 eV) and second overtone (at 0.571 eV) are observed. The inelastic tails extend to higher loss energies indicating a combination of the stretching mode and another lower-lying loss. The excitation mechanism was identified [36] as a negative ion resonance (NIR) involving the ${}^4\Sigma_u^-$ shape resonance of O_2. The spectrum exhibits all typical signs of NIR [64] which are (1) high intensity of overtone excitation of the stretching mode, (2) strong inelastic tails of the vibrational modes and the elastic peak and (3) high scattering intensity out of the specular angle. (1) and (2) are clearly recognized in figure 5. (3) is also evident from the fact that the spectrum in figure 5 is measured 30° off the specular direction. The stretching mode ($n = 0 \rightarrow n = 1$) is observed at 192.4 meV near to the gas phase value of 194 meV.

In the anharmonic-oscillator model, the loss energy ΔE associated with the vibrational overtones is related to the vibrational frequency ω and the anharmonicity ωx of the anharmonic oscillator by the equation $\Delta E_{(v=0\rightarrow v=n)} = n\omega - n^2\omega^2 x^2$ [65]. The dissociation energy of the Morse oscillator is given by $D = -(\omega + \omega x)^2/4\omega x$. We find $\omega = 194.4 \pm 0.3$ meV, $\omega x = -1.6 \pm 0.2$ meV and $D = 5.8 \pm 0.6$ meV. These values are in agreement with values obtained for O_2 on polycrystalline Ag [65].

For the O_2 multilayer (see figure 9 below), as prepared by dosing with 10 L O_2, the spectrum of figure 5 changes slightly as can be seen from figure 9 discussed below in the context of O_3 formation: according to a—compared with the gas phase—less reduced lifetime of the NIR, the inelastic tails to higher energies are more intense. Furthermore, there is a structure at 7 meV below the stretching mode indicative of contributions from translational modes. The ${}^4\Sigma_u^-$ shape resonance energy for the multilayer is depicted in figure 6. It's peak at an incidence energy of 9 eV is near to the value of 9.5 eV found for the gas phase [66]. Within the experimental error it is independent of the angle of incoming and outgoing electrons. Our curve is in very good agreement with that reported by Tang *et al* [67] for Ag(110) (see figure 11).

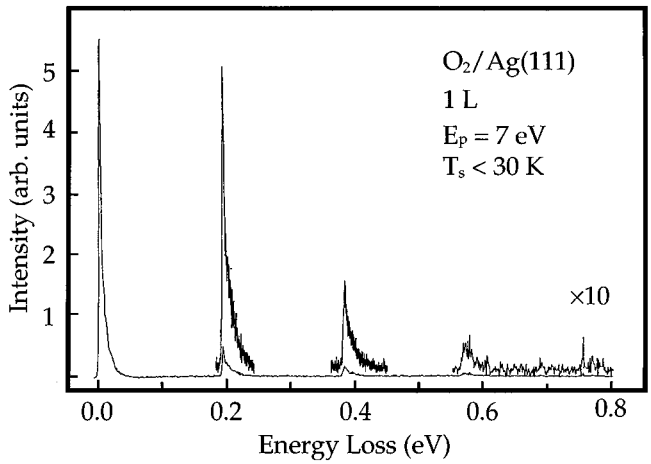

Figure 5. HREEL spectra for 1 Langmuir (1.33×10^{-6} mbar × s) O_2 physisorbed on Ag(111) at a temperature T_s below 30 K. The primary energy E_p is indicated. Angle of incidence $\theta_i = 75^\circ$ and angle of emission $\theta_e = 45^\circ$, both with respect to the surface normal. From [36].

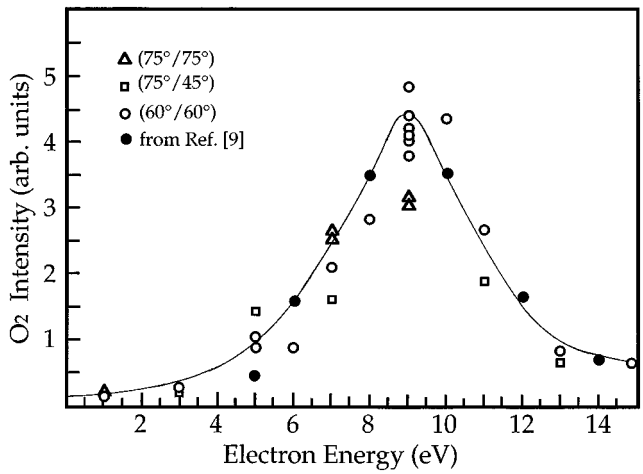

Figure 6. O_2 stretching mode ($n = 0 \rightarrow 1$) intensity ($\bar{h}\omega = 193$ meV) versus energy of the incident electrons. The data are for three different couples of incidence and emission angles (relative to the surface normal). The intensity is normalized against the background on the left side of the O_2 stretching mode.

These authors also found the same curve shifted to lower energies by 2 eV for the O_2 monolayer due to interaction with the Ag(110) surface. We have not measured this curve for Ag(111).

Despite the high-energy resolution, the inelastic tail was not resolved into single vibrational or rotational modes. This can be seen more clearly in a narrow energy scan around the vibrational mode depicted in figure 7(c). A similar observation was made for N_2 physisorbed on Ag(111) shown in figure 7(b). For comparison an earlier spectrum is shown in figure 7(a) [68]. At that time it was believed that the N_2 vibrations against the surface were not resolved due to a limited energy resolution. The same conclusion was drawn for N_2 on Al(111) [69]. Compared with Ag(111) the inelastic tail was found to be more intense than the N_2 vibrational mode for Al(111) [69].

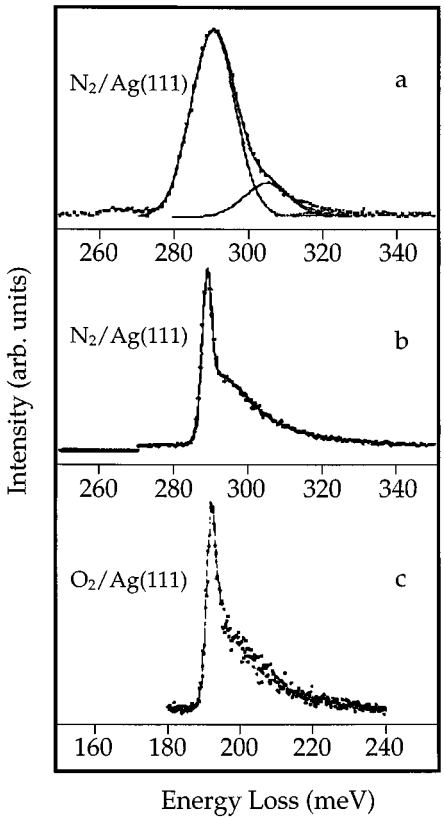

Figure 7. HREEL spectra around the ($n = 0 \rightarrow 1$) stretching mode for: (a) N_2 on Ag(111) from [68]; (b) N_2 on Ag(111) at better energy resolution from [70]; (c) O_2 on Ag(111) from [36].

The formation and deexcitation of the $^4\Sigma_u^-$ resonance are due to the capture (and emission) of an electron with pσ ($l = 1$) and fσ ($l = 3$) symmetries [71]. In each step the total angular momentum of the system is conserved, giving the selection rules for the target molecule rotational state j $\Delta(j) = \pm 1$ and $\Delta(j) = \pm 3$ in the gas phase respectively for $l = 1$ and $l = 3$. The selection rules that apply to the two-step rotational excitation of O_2 ($j = 0 \rightarrow j' \geqslant 0$) through the $^4\Sigma_u^-$ resonance are: $\Delta(j) = 0; \pm 2; \pm 4; \pm 6$. The ratios between the different series are not calculated yet. Moreover, O_2 which is a boson of nuclear spin equal to 0, admits exclusively a rotational population with odd j [72]. Considering the rotational constant equal to $B = 0.18$ meV [72], we calculated the theoretical energy spectrum of the pure rotational excitation of O_2 in the gas phase (at 25 K) as shown in figure 8. This does not display any intense structure in the range 6–8 meV. Hence the shape of the experimental loss peaks cannot be fully explained as being solely due to pure rotational excitation of the molecule. This result is also supported by the fact that the peak shapes of the overtones are different from each other, contrary to what is expected if the shape were only due to the initial population (j) of O_2.

Although the inelastic tail could not be resolved into individual losses, it is very likely that translational modes with energies of 6–8 meV are involved in establishing the tail. This conclusion is drawn due to the large width of the tails, the negligible intensity gain (to the left of the stretching mode) and one resolved structure of about this energy for the O_2 multilayer.

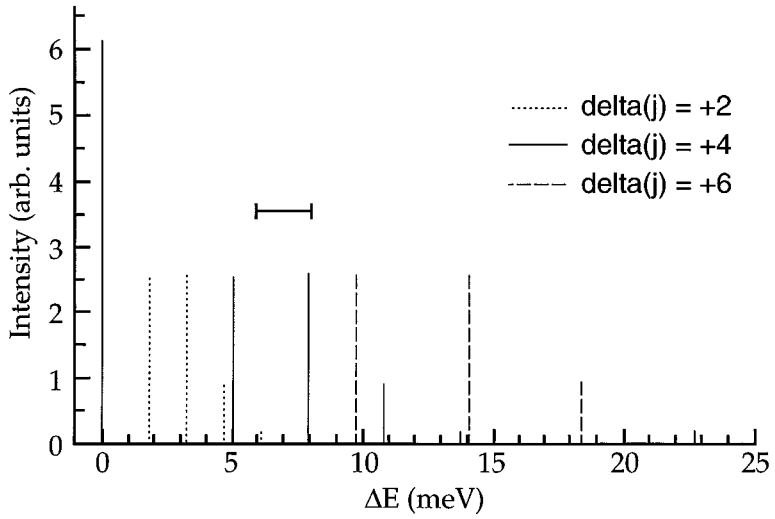

Figure 8. Theoretical spectrum of the pure rotational excitation of O_2 in the gas phase at 25 K. The horizontal error bar at 6 to 8 meV gives the energy at which a peak in the experimental spectra was found.

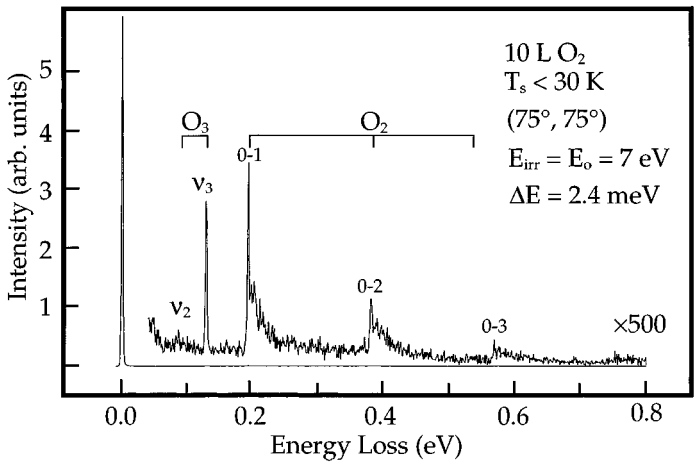

Figure 9. HREEL spectra for a O_2 multilayer according to a O_2 dose of 10 L. Substrate temperature T_s, angle of incidence and emission, energy of the electrons E_{in} during irradiation of the film for about 8 h at 30 pA, electron energy for taking the HREEL spectra E_0 and energy resolution ΔE (FWHM) are given. O_2 and O_3 losses are indicated.

In summary, the O_2/Ag(111) physisorption system displays similar vibrational properties to those observed for N_2/Al(111) [64, 69], i.e., for a homonuclear molecule, which does not exhibit a dynamic dipole moment in the physisorbed case on an sp-metal surface. For physisorption of heteronuclear molecules, like CO/Al(111) [64, 69] and CO/Ag(111) [73], dipole scattering prevails at monolayer coverages.

Finally, it may be interesting to note that ozone formation was observed under the influence of the irradiating electron beam of the HREEL spectrometer for an O_2 multilayer on Ag(111) [74]. Figure 9 shows a multilayer spectrum after irradiation with electrons at a primary energy

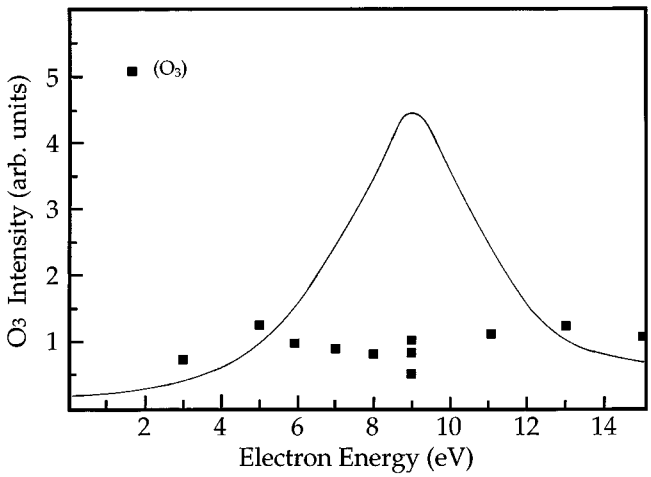

Figure 10. Intensity of the ν_3 (asymmetric stretching) mode as a function of the energy of the incident electrons (full squares). The full line is for the $^4\Sigma_u^-$ shape resonance of physisorbed O_2 from figure 6.

of 7 eV and a current of 30 pA for about 8 h. Besides the O_2 derived losses, as known from figure 5, a very sharp loss at $\nu_3 = 128.6$ meV is observed. The peak at $\nu_2 = 86$ meV is better resolved after reducing the energy of the primary electron beam to 3 eV. These lines are assigned to O_3, ν_3 being the asymmetric stretching mode and ν_2 the bending mode of O_3, and are in very good agreement with EELS measurements for gas-phase O_3 [75]. It is also worth noticing that the presence of O_3 has also been proven by electron stimulated O^- desorption [74]. Both peaks are dipole active; this can be verified by changing the measuring angle and by the dependence on the impact energy which is shown in figure 10. One clearly recognizes that the excitation does not show any clear resonance. The slight antiresonance around 9 eV may be due to the normalization procedure. Actually, one should subtract first the part of the primary electrons which is responsible for the NIR channel. This would reduce the intensity of the elastic peak which is used to normalize the dipole active modes thus increasing the normalized intensity of the dipole mode. This example demonstrated that NIR is also very helpful in identifying unknown physisorbed species as, in addition to the NIR scattering from O_2, dipole scattering from O_3 is observed.

4. O_2/Ag(110): physisorption

The scattering properties of an electron by a molecule are dominated by the formation of molecular negative ion intermediates. Such resonant processes play a very important role in the energy transfer from an electron to a molecule, leading very efficiently to the electronic and/or vibrational excitation of molecules. A wealth of information (energy position, lifetime, symmetry) on negative ion resonances was accumulated for free molecules in the 1970s [42] and more recently for adsorbed molecules [40, 41, 64] using the high-resolution electron energy loss spectroscopy (HREELS) technique. It has been shown that the resonances observed for physisorbed molecules can be associated with those observed for free molecules, however with their characteristics modified by the metal environment. Section 4.1 will consider the modification of resonance energy position and lifetime due to the physisorption and section 4.2 will focus on the angular behaviour of the resonant electron scattering.

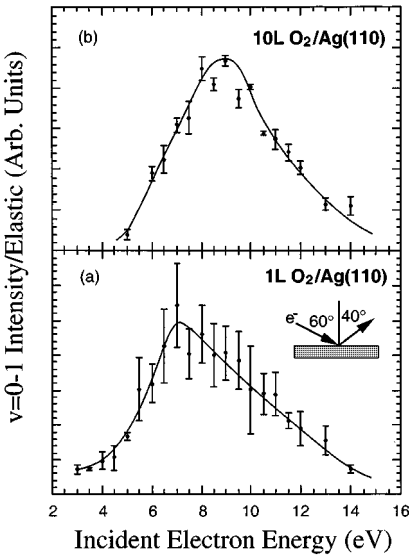

Figure 11. Resonance energy profiles obtained from physisorbed O_2 on Ag(110) at $T = 20$ K. The experimentally observed intensity of the 190 meV $v = 0 \rightarrow 1$ vibrational excitation of the O_2 molecule, normalized to the diffuse elastic intensity, is plotted as a function of the incident electron energy. The incident angle is 60° and the detection angle is 40° in both cases. Resonances are observed at (a) 7 eV for an O_2 dose of 1 L, and (b) at 9 eV for an O_2 dose of 10 L. The solid curves are drawn as a guide to the eye.

4.1. Resonance energy and lifetime

This section examines how the formation of negative ion resonances is exploited, via the HREELS technique, to study the resonance characteristics of oriented physisorbed O_2 molecules on the Ag(110) surface. The focus is on the resonance energy and lifetime, as a function of the structure of the adsorbed layer. Resonance energy shifts in physisorbed molecules [41], e.g. O_2 physisorbed on graphite [76, 77], a semi-metallic substrate, are now well established. Previous studies of the resonance lifetime in physisorbed monolayers also indicated significant changes with respect to the gas-phase resonance lifetime [41, 78, 79]. It is therefore valuable to explore the precise mechanisms by which these fundamental parameters of the resonance state are perturbed on a well defined Ag(110) surface. The experimental results are compared with theoretical calculations which employ the layer-Korringa–Kohn–Rostoker (LKKR) model [80–84] to predict the resonance energy and lifetime of an adsorbed molecule as a function of adsorption height.

HREELS measurements of physisorbed O_2/Ag(110) were performed for both monolayer and multilayer coverages, corresponding to 1 L and 10 L exposures, at 20 K. The experimental details can be found in [67]. Typical HREEL spectra show that the $v = 0 \rightarrow 1$ vibrational excitation of the physisorbed O_2 molecule is manifest as a peak in the HREEL spectra at an energy loss of 190 ± 5 meV [67]. This value is approximately the same as that observed in the gas phase [66] and on both Pt(111) [85], Ag(111) [36] and graphite [77], and is an indication that the O_2 molecule is only weakly perturbed on adsorption. Intense vibrational overtone excitations, which are characteristic of the resonant excitation mechanism and arise from the relatively long lifetime of the electron–molecule interaction, are also observed [36, 67].

The intensity of the $v = 0 \rightarrow 1$ loss peak was monitored as a function of the incident electron energy and normalized to the diffuse elastic intensity [41] to give the resonance energy profile for the vibrational excitation of physisorbed O_2/Ag(110). The resulting energy dependence, for both monolayer and multilayer coverages of O_2, is shown in figures 11(a) and (b). As the O_2 dose is increased, the well defined resonance centred at $\approx$7 eV in figure 11(a) is shifted to higher energy, with a peak at $\approx$9 eV in figure 11(b). This resonance is assigned to the $^4\Sigma_u^-$ negative ion state, which is formed by adding an electron to the lowest unoccupied 2p σ_u^*

orbital of the O_2 $^3\Sigma_g^-$ ground state, and is observed at an energy of about 9.5 eV in the gas phase [66]. The shift in resonance energy is attributed to the effect of the image potential, which has similarly been observed on graphite [76, 77] and Pt(111) [85]. This conclusion is in agreement with prior theoretical studies by Gerber and Herzenberg [86] as well as the coupled angular momentum (CAM) calculations of Teillet-Billy *et al* [87, 88], and is confirmed by a recent study [67] which employed the LKKR method [80–84] to take into account any influence of the substrate atomic potential. The results of the LKKR calculations showed that the resonance energy varies as the surface barrier (image) potential, independent of the adsorption site, and is thus largely unaffected by the unoccupied electronic states of the substrate [67]. Therefore, the reduction of the energy of the negative ion upon physisorption is primarily a consequence of the electrostatic screening of the negative ion.

The resonance lifetime, although accessible to HREELS, cannot be measured directly. Rather, the change in the relative overtone intensities as a function of exposure reflects the lifetime of the O_2^- resonance state. Thus, if the resonance lifetime of a molecule, t_R, is altered by adsorption, then this will be manifest in the rate of decay of the intensity of the loss features as a function of the overtone number. A decrease in the resonance lifetime will cause the vibrational overtones to decay more rapidly than for the free molecule, whilst an increase of the resonance lifetime will tend to have the opposite effect.

An analysis of the decay of the vibrational overtone intensities to extract the lifetime of O_2 physisorbed on Ag(110) was performed [67, 78, 79]. The analysis employs the displaced harmonic oscillator model proposed by Gadzuk [78, 79], which was employed previously to estimate the lifetime of the $^2\Pi_g$ resonance (2.3 eV) of N_2 physisorbed on polycrystalline Ag [78, 79]. In figure 12(a) we show the overtone intensities computed by using the displaced harmonic oscillator model described above, plotted as a function of the resonance lifetime (expressed as a percentage of the lifetime of the free molecule $= 100\%$). Also shown are the loss intensities (after background subtraction) of the $v = 0 \rightarrow 2$ and $v = 0 \rightarrow 3$ overtones, normalized to the $v = 0 \rightarrow 1$ transition, measured for both monolayer and multilayer coverages of O_2 on Ag(110).

Figure 12(a) also includes the measured decay of the overtones for the free molecule, as measured by Wong *et al* [66]; good agreement is obtained with the predictions of the displaced harmonic oscillator model. For both the 1 and the 10 L coverages of O_2 physisorbed on Ag(110), we observe that the measured overtone intensities decay more rapidly than those for the molecule in the gas phase. This feature, which has also been observed in the loss spectrum for resonance scattering by N_2 on polycrystalline Ag [78, 79], indicates that the resonance lifetime is reduced upon adsorption and that the resonance lifetime is shorter for a coverage of 1 L (the monolayer) than for 10 L (the multilayer). The coverage effect on the overtone excitation has been calculated in the N_2 case [88]. The calculation using the CAM method shows that the overtone excitation strongly depends on the adsorption height and decreases when this height is decreased. From figure 12(a) we observe that the calculated rate of decay of the overtone intensities from the physisorbed molecule at 1 L coverage is in excellent agreement with the measured intensities, if the resonance lifetime of the adsorbed molecule is reduced to $70 \pm 10\%$ of the lifetime of the free molecule. The lifetime reduction for 10 L coverage is significantly smaller; in this case, the lifetime of the adsorbed molecule is $90 \pm 10\%$ of the lifetime of the free molecule. These results suggest that the negative ion state in adsorbed O_2 is more strongly quenched in the monolayer than in the multilayer.

Figure 12(b) shows the resonance lifetime computed by the LKKR method for the O_2 molecule adsorbed parallel to the Ag(110) surface. The calculated lifetime of the resonance is plotted as a function of the adsorption height of an isolated molecule above the twofold hollow site, and shows distinctive oscillations. For the monolayer phase, the LKKR calculation of the

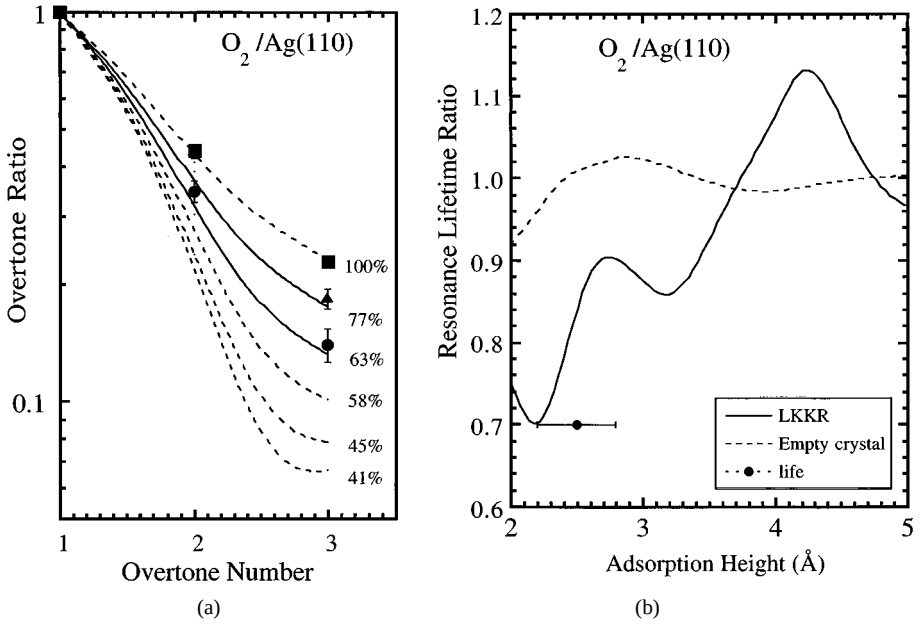

Figure 12. (a) Overtone intensities in resonance electron scattering by O_2 (via the $^4\Sigma_u^-$ resonance) plotted as a function of the overtone number and normalized to the $v = 0 \rightarrow 1$ loss. Filled squares: overtone intensities for the free molecule measured by Wong *et al* [66]. Filled circles: overtone intensities for 1 L of O_2 physisorbed on Ag(110). Filled triangles: overtone intensities for 10 L of O_2 physisorbed on Ag(110). The dashed curves are calculated overtone intensities obtained from the displaced harmonic oscillator model, where the resonance lifetime (labelled as a percentage of the lifetime of free O_2) is treated parametrically. The solid curves indicate the upper and lower bounds of the resonance lifetime that are consistent with the experimental data for physisorbed O_2 at 1 L coverage. (b) The relative resonance lifetime (1.0 = gas phase lifetime) of the $^4\Sigma_u^-$ shape resonance of O_2, evaluated by a layer-KKR calculation, plotted as a function of the adsorption height of the molecule. Solid curve: full LKKR calculation, including full multiple scattering of the trapped electron by the substrate. Dashed curve: the empty crystal approximation where only the image interaction between the negative ion and the metallic substrate is included. Solid circle: the resonance lifetime determined for 1 L coverage of the physisorbed molecule corresponding to an adsorption height of 2.5 ± 0.3 Å.

resonance energy as a function of the molecular adsorption height suggests (after comparison with the experimental resonance energy) that the molecule is adsorbed 2.5 ± 0.3 Å above the first atomic plane of Ag(110) [67]. From figure 12(b), we see that an O_2 molecule adsorbed at this height has a calculated lifetime of $80 \pm 10\%$ compared with the lifetime of the negative ion in the free molecule. This reduction of the lifetime is in reasonable agreement with the resonance lifetime extracted from the measured decay of the overtone intensities, $70 \pm 10\%$.

When the lifetime is computed for an empty crystal, also shown in figure 12(b), we see that there is almost no variation in lifetime over a range of realistic adsorption heights. The empty crystal neglects any electron scattering among the substrate atoms and considers only the image interaction between the negative ion and the metallic substrate, a strategy adopted by the CAM method. Qualitatively, the surface barrier potential of Ag, estimated from the sum of the Fermi energy and the work function of the metallic substrate, is about 9.8 eV [86]. The incident energy of the probe electron, corresponding to the $^4\Sigma_u^-$ negative ion state of O_2, is comparable with this barrier height. Therefore, the probe electron would not be strongly

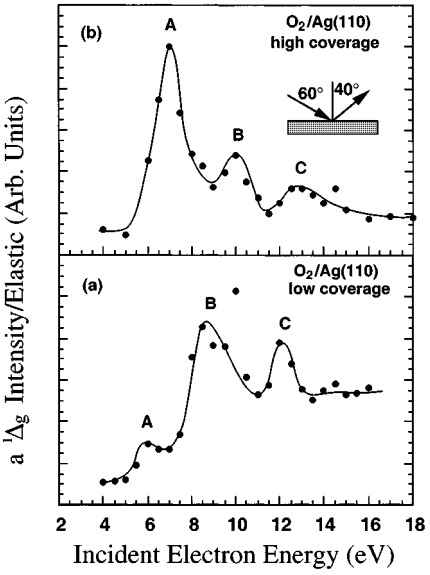

Figure 13. Resonance energy profile for the $X^3\Sigma_g^- \rightarrow a^1\Delta_g$ electronic excitation, normalized to the diffuse elastic intensity, from O_2/Ag(110) at $T \sim 20$ K. The incident angle is 60° and the detection angle 40°. Resonances are observed at incident energies of (a) 6, 8.5 and 12 eV in the low-coverage regime, and (b) 7, 10 and 13 eV in the high-coverage regime, respectively.

scattered by the surface barrier and would be expected to interact predominantly with the unoccupied electronic band structure of the crystalline substrate.

Resonance states are not only manifest in the cross-sections for vibrational excitation of molecules but also in electronic excitation. HREELS was employed to study the $X^3\Sigma_g^- \rightarrow a^1\Delta_g$ electronic excitation of O_2 molecules physisorbed on Ag(110) [89]. The $X^3\Sigma_g^- \rightarrow a^1\Delta_g$ excitation, evident as a peak in the HREEL spectrum at 975 ± 5 meV, was monitored as a function of the incident electron energy. The results are shown in figure 13. Three resonances, peaks A, B and C, were observed to occur at incident electron energies of $\approx$7, 10 and 13 eV in the multilayer regime, figure 13(a), and shifted to lower energies by about 1–1.5 eV in the monolayer, figure 13(b). This perturbation of the resonance energy of the negative ion state by the metallic Ag(110) surface is consistent with the discussion above, and therefore is again believed to arise from image potential screening.

It is interesting to further note that the relative intensities of these peaks also change dramatically as a function of coverage, figure 13, possibly reflecting a modification in the relative lifetimes of the resonances. Since peaks B and C were not seen in earlier gas phase studies, the appearance of these resonant states is of particular significance and can be compared with similar features observed in electron stimulated desorption (ESD) studies of condensed O_2 [90–92]. These ESD studies reported two resonances at 9 and 13 eV, whose appearance was attributed to the violation of the $\Sigma^+ \rightarrow \Sigma^-$ symmetry selection rule through O_2–O_2 coupling [90, 93]. However, in figure 13, peaks B and C are enhanced, compared with peak A, in the monolayer regime rather than in the multilayer where the O_2–O_2 interaction would be strongest. An intuitive explanation for this observation would be that the O_2–surface interaction is responsible for enhancing the B and C resonances. Rous [82] has shown that the lifetime of a negative ion can be *increased* upon adsorption, when the effects of the substrate electronic states on the resonance scattering are taken into consideration. We have seen, figure 12(b), the dramatic effect that the interaction between the molecular resonance state and the unoccupied electronic states of the surface has on the resonance lifetime. Moreover, Sambe *et al* [94] have reported an increase in the cross-section for molecular dissociation via electron capture on the surface compared with the gas phase, due to the quenching of

intramolecular electronic deexcitation of the resonance state [94]. Therefore, the argument for enhanced lifetime in the monolayer offers a plausible alternative explanation of the appearance of peaks B and C.

In conclusion, HREELS measurements reveal that both the resonance energy and lifetime of the negative ion states of O_2 is dependent on coverage on the Ag(110) surface. The downward shift in resonance energy from the multilayer regime to the monolayer regime is attributed to the effect of the image charge potential. The perturbation of the resonance lifetime, however, is found to be more complicated, and depends critically on the interaction of the resonance state with the unoccupied electronic states of the substrate.

4.2. Angular distribution of resonant electron scattering by oriented physisorbed molecules: study of the O_2/Ag(110) system

There is a correspondence between the resonances for free molecules and for physisorbed molecules. However, the change in the molecular environment modifies the characteristics of the resonant scattering, as discussed for the overtone excitation in the previous section. The angular properties of the resonant scattering for physisorbed molecules will be discussed here. For free molecules, the angular behaviour of the inelastically scattered electron only depends on the molecular asymmetry of the intermediate state: the symmetry assignment is obtained from the analysis of the electron angular distribution [95]. The electron angular distribution directly reflects the molecular symmetry of the resonance, averaged over the free orientation of the molecule in space. The angular analysis makes use of a very small number of partial waves (one or two) to describe the angular behaviour of the incident and emitted electron scattering in the case of low-energy resonances. On a surface, the adsorbed molecule is often oriented, the orientation being held fixed by the molecule-to-substrate and molecule-to-molecule interactions. For physisorbed molecules, the angular distribution of scattered electrons is then expected to reflect not only the symmetry of the resonant state (known from the gas phase studies but which may be perturbed by adsorption) but also the orientation of the molecular axis, and consequently it can probe both these aspects [96–98]. Our purpose here is to present and discuss the relevance of an electron emission angular study for the determination of the orientation of adsorbed molecules. The present theoretical study is based on a classical model for the electron scattering that takes into account the orientation of the molecular axis, both in azimuthal (in-plane) and polar (out-of-plane) orientation with respect to the surface. We will show that the angular properties of the electron emission strongly depend on the orientation of the molecular axis and that an angular study as a function of both the azimuthal and polar angles can provide a three-dimensional view of the oriented molecule, helpful for the structure determination. The present paper focuses on what can be learned on one particular system of interest—O_2 molecules physisorbed on a silver substrate—by the use of the specific properties of resonant inelastic electron scattering. The O_2/Ag(110) system is of particular interest since, according to a near-edge x-ray-absorption fine-structure (NEXAFS) study [103], the adsorbed molecules have a well defined orientation, both in azimuthal and polar angles, with respect to the Ag crystal. We will present below the case of the angular distribution of electrons resonantly scattered by O_2 molecules physisorbed by Ag(110) via the $^4\Sigma_u^-$ resonance. Our study shows that the structural changes with coverage (from the monolayer to the multilayer regime) can be followed quantitatively by the change in the angular distributions of resonantly scattered electrons, with a satisfactory agreement with the previous determination of the structural parameters by the x-ray absorption technique. This work confirms the possible use of resonant electron scattering and of its angular properties as a relevant tool for structural analysis of physisorbed species.

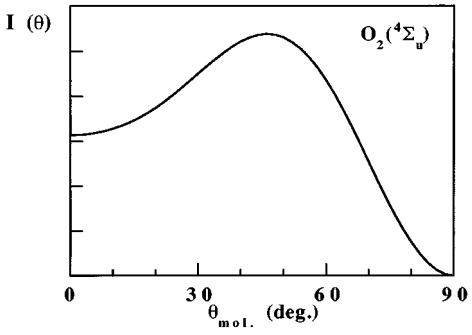

Figure 14. Angular part of the σ_u orbital involved in the formation of the $^4\Sigma_u^-$ resonance of O_2; it is represented by a superposition of pσ and fσ waves that has been adjusted to represent the experimental results on the free molecule [103]. The angle is relative to the molecular axis.

The theoretical model for the angular distribution of resonantly scattered electrons takes into account: (i) the angular shape of the resonant wavefunction, which determines the resonant capture and emission probabilities as functions of the relative position of the electron emission (capture) direction and of the molecular axis, (ii) the possible distribution of orientations of the molecular axis and (iii) the effect of the refraction due to the image potential of the substrate on the incident and outgoing electrons. It considers the differential cross-section as a product of two transition probabilities, one for the attachment step and one for the detachment. A single molecule is considered in the present approach and multiple scattering effects due to the neighbouring adsorbates are not included. The coherent aspect of multiple scattering has been considered in the case of O_2 on graphite [99, 100].

In the present case, the angular shape of the $^4\Sigma_u^-$ resonance of O_2 is represented as a superposition of pσ and fσ waves (with relative amplitudes 1 and 0.4) chosen to fit the most recent experimental angular results [101] on free molecules. The angular part of the resonant σ_u wavefunction is presented in figure 14, with the polar angle relative to the molecular axis. The wavefunction presents one node in the direction perpendicular to the molecular axis, characteristic of a σ_u orbital.

In the present study, we only consider experimental situations where the incident and outgoing electron trajectories are in the same plane normal to the surface, called the scattering plane. Different orientations of the molecule and of the scattering plane are considered. The scattering plane is defined by the azimuthal angle ϕ (angle between the scattering plane and the plane normal to the surface containing the molecular axis). For the molecule polar orientation, we will consider different physical situations, either a molecule with a fixed polar angle (Γ^0: angle between the molecular axis and the surface), or a distribution of polar angles ($\Delta\Gamma^0$) that corresponds to a frustrated polar motion with a uniform distribution of molecular orientation over the $\Delta\Gamma^0$ range. The refraction arising from the image potential is treated classically [102]. The value of the image potential is obtained from the energy shift of the resonance as measured by electron scattering experiment on O_2/Ag(110) [71]: the downward shift energy is 2.5 eV (0.5 eV) for monolayer (respectively multilayer) physisorption. This refraction effect is included both for the incident and outgoing electrons.

Figure 15 shows the calculated angular distribution of electrons scattered via the $^4\Sigma_u^-$ resonance of O_2 for various physical situations: a molecule with either an in-plane orientation $\Gamma = 0^\circ$ (molecule parallel to the surface plane) (figure 15(a)) or an out-of-plane angle $\Gamma = 30^\circ$ (figure 15(b)). The figure presents the angular distributions in the scattering plane as function of θ, the polar angle (measured from the surface normal) for the different positions of the scattering plane (ϕ: azimuthal angle between the scattering and molecular planes). In all cases, the incident electron direction is at 60° from the surface normal, which corresponds to the experimental conditions [71].

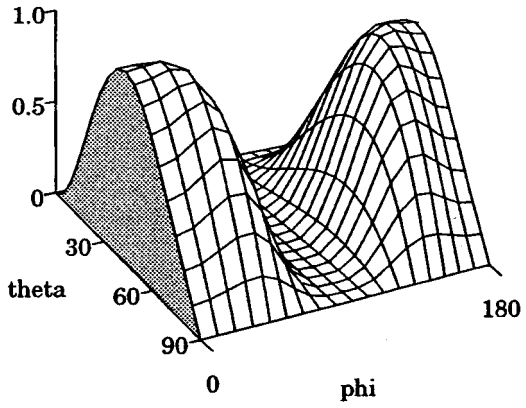

(a)

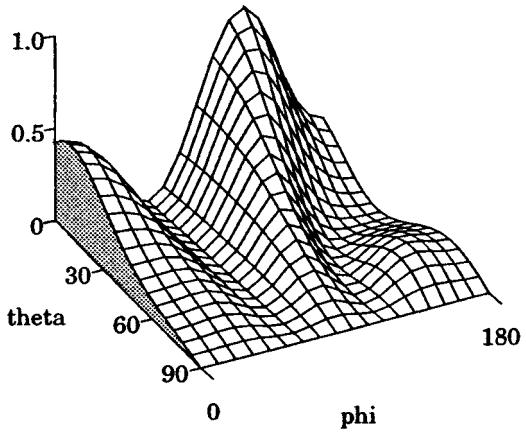

(b)

Figure 15. Calculated angular distributions of electrons ejected by the $^4\Sigma_u^-$ resonance of O_2, represented by a superposition of pσ and fσ waves, for O_2 physisorbed on a metal as a function of the polar angle of emission (θ), for different azimuthal angles (ϕ) between the scattering plane and the molecular axis. The polar orientation of the molecular axis is either parallel to the surface plane ($\Gamma = 0^\circ$)—figure 15(a)—or with an out-of-plane orientation tilt angle $\Gamma = 30^\circ$—figure 15(b). The downward image charge energy shift corresponds to the monolayer regime.

The angular distributions of the scattered electrons are found to be very different for the different orientations of the scattering plane and to strongly depend on the polar orientation of the molecular axis (figures 15(a) and (b)). This is expected since the capture and emission cross-sections depends on the relative angles of the incident and outgoing electrons with respect to the molecular axis. The emitted electron distributions are different for the two outgoing azimuthal angles $\phi = 0$ or $\phi = 180^\circ$ in the case of an out-of-plane orientation of the molecular axis: these two situations correspond to two different geometries of incidence and emission relative to the molecular axis. The distribution corresponding to $\phi = 90^\circ$ vanishes for the in-plane orientation of the molecule (figure 15(a)): this is a consequence of the σ_u character of the resonant orbital, which presents a node in the plane normal to the molecular axis. This property shows up at a different azimuthal angle for an out-of-plane orientation of the molecule. The vanishing distribution for a detection polar angle of

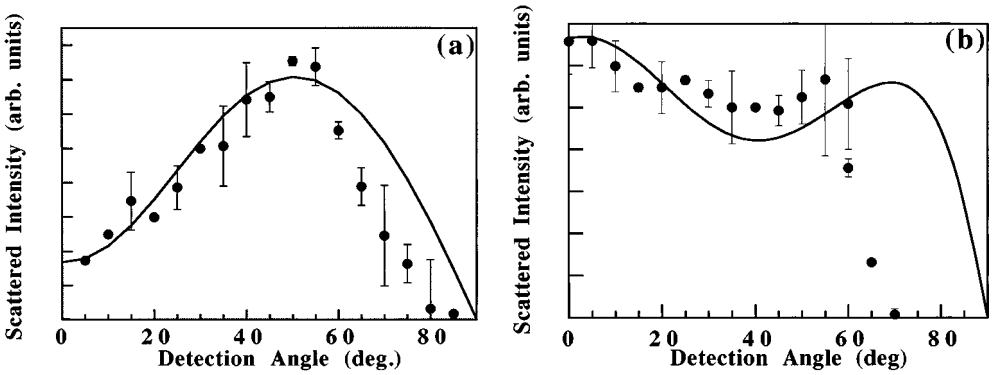

Figure 16. Comparison between the experimental angular distributions for physisorbed O_2/Ag(110) (filled circles with error bars) and calculated distributions (full line) which use the orientational parameters derived from NEXAFS experiments [103]. (a) Monolayer coverage regime [71]. Calculated distribution (——): the azimuthal angle, ϕ, is 30°, the mean orientation of the molecular axis is parallel to the surface plane ($\Gamma = 0°$) and the molecule executes a frustrated rotation given by $\Delta\Gamma = \pm 20°$. (b) Multilayer coverage regime [71]. Calculated distribution (——): the azimuthal orientation of the molecular axis is fixed ($\phi = 30°$), the molecule is tilted away from the surface ($\Gamma = \pm 30°$) and the molecule executes a frustrated rotation given by $\Delta\Gamma = \pm 15°$.

90° (i.e. parallel to the surface plane) is common to all the distributions; it is due to the image charge potential [102] that generates a node in the surface direction for any resonance symmetry.

Strong coverage effects have been observed by x-ray absorption [103] and by electron scattering for the O_2/Ag(110) system, in the energy range corresponding to the $^4\Sigma_u^-$ resonance [71]. This clearly demonstrates that resonant electron scattering studies are sensitive to changes in structural properties of adsorbed molecules. The experimental angular distribution for the monolayer (figure 16(a)) and for the multilayer case (figure 16(b)) shows several distinctive features: a minimum along the sample normal in the monolayer case in contrast to the multilayer case which presents a substantial signal in the direction of the surface normal [71]. These features can be interpreted qualitatively and quantitatively by our model. According to the σ_u symmetry of the intermediate state (see figure 14), the minimum along the surface normal clearly indicates a molecular orientation approximately parallel to the surface in the monolayer and the absence of the node normal to the surface plane in the angular distribution from the multilayer suggests a departure from the lying down orientation. This qualitatively agrees with the NEXAFS study [103].

Using our model, we have calculated the angular distributions in resonant electron scattering by physisorbed O_2/Ag(110) based on the conclusions of the NEXAFS study with the incident and exit angles corresponding to the experimental electron scattering geometry. The electron experiment has been performed as a function of the exit polar angle but for only one scattering plane. We have considered, according to the NEXAFS conclusion, a molecular axis perpendicular to the Ag rows and thus the azimuth angle ϕ—the angle between the experimental collision plane and the plane normal to the surface containing the molecular axis—is equal to 30°. In the case of the monolayer, a good agreement with electron scattering experimental results is obtained for a mean in-plane orientation of the molecular axis (tilt angle $\Gamma = 0°$) with a distribution of tilt angles away from the surface ($\Delta\Gamma = \pm 20°$) (figure 16(a)). The small distribution of out-of-plane tilt angles is responsible for the weak signal in the direction

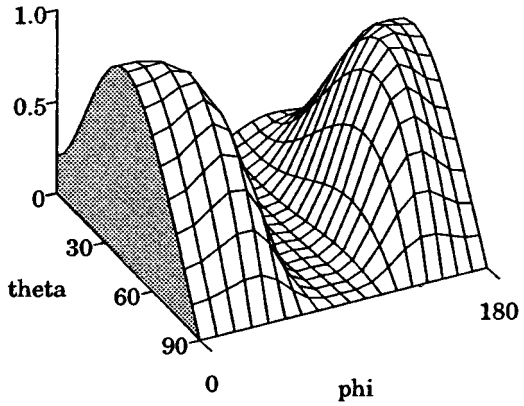

(a)

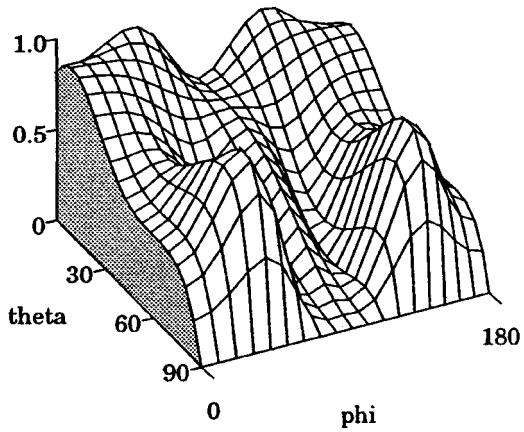

(b)

Figure 17. Calculated angular distributions of electrons ejected by the $^4\Sigma_u^-$ resonance of O_2 for different azimuthal angles between the scattering plane and the molecular axis when a frustrated motion is taken into account. (a) Polar orientation of the molecular axis ($\Gamma = 0^\circ$, with $\Delta\Gamma = \pm 20^\circ$). (b) Polar orientation of the molecular axis ($\Gamma = \pm 30^\circ$, with $\Delta = \pm 15^\circ$). The downward image charge energy shift corresponds to the monolayer (multilayer respectively) regime for (a) ((b)). These figures correspond to the calculated three-dimensional shape of the angular distribution, in polar and azimuth angles, for the electron emission. Figures 16(a) and (b) correspond to the cut at $\phi = 30^\circ$.

of the surface normal. For the multilayer regime, the distribution of figure 16(b) is obtained for molecules again normal to the surface troughs ($\phi = 30^\circ$) and tilted away from the surface plane. The agreement is obtained for an out-of-plane angle $\Gamma = \pm 30^\circ$ that takes into account the two equivalent up and down direction of tilt and a frustrated tilt of $\Delta\Gamma = \pm 15^\circ$, that excludes the in-plane orientation. This conclusion is consistent with the NEXAFS study [103] which concludes that the molecules progressively align more towards the surface normal with increasing coverage. In the present model, the enhancement of the angular distribution at a detection angle of around 60°, figure 16(b), comes from the shape of the $^4\Sigma_u^-$ resonant orbital. The angular distribution of resonantly scattered electrons thus appears to be a powerful method to address the problem of the orientation of physisorbed molecules as part of the structural properties of an adsorbed layer.

The angular distributions reflect the three-dimensional shape of the resonant orbital as shown in figure 15. However, an experiment performed with a fixed azimuthal angle ϕ (as in the present case) only looks at a cut through this orbital and this could lead to ambiguities. The frustrated motion in polar angles has appeared as an important parameter to interpret quantitatively the experiments and one many wonder if the three-dimensional information presented in figure 15 is not smoothed away by the frustrated polar motion. Figure 17 presents the three-dimensional view of the angular distributions of the emitted electron for physical conditions similar to the experimental ones. As in figure 15, the angular distribution in the scattering plane is given as a function of θ for different positions of the scattering plane (ϕ). In figures 17(a) and (b) the same frustrated motion in polar angles as in figure 16 has been taken into account (figure 17(a) corresponds to $\Gamma = 0^\circ$, $\Delta\Gamma = \pm 20^\circ$ and figure 17(b) to $\Gamma = \pm 30^\circ$, $\Delta\Gamma = \pm 15^\circ$). Figure 17 shows that even with this frustrated polar motion, the anisotropy of the electron scattering by the molecule can still be clearly analysed by an angular study. A three-dimensional analysis of the angular distribution, in both azimuthal and polar angles, would be useful to extract orientational properties of adsorbed molecules.

We have presented a theoretical model for angular distributions in resonant electron scattering: it has been applied to the electron scattering by physisorbed O_2 on Ag(110) involving the $^4\Sigma_u^-$ resonance. The change in the molecular orientation as the O_2 coverage is increased from the monolayer to the multilayer regime can be followed by an angular distribution study of the electron emission. The model calculation quantitatively confirms the orientation of the O_2 molecule as determined by an x-ray absorption study [103]: the molecule lies approximately parallel to the surface and perpendicular to the rows of atoms on the Ag(110) in the monolayer regime and is substantially tilted away from the surface in the multilayer. The present results show a very strong dependence of the angular distributions of resonantly scattered electrons on the geometrical properties of the molecule–surface system: relative position of the molecular and scattering planes, relative molecule–surface orientations. This confirms the capability of the HREELS angular analysis for providing geometrical information on adsorption systems. Indeed, an unambiguous assignment of the adsorbed molecule orientation can only be extracted from measurements involving both polar and azimuthal angles. Experiments of this kind would helpfully contribute to the analysis of adsorbed molecules.

5. NIR of physisorbed and chemisorbed states of O_2 on Ag(110)

This section examines the adsorption of oxygen on Ag(110) at 15 and 75 K studied by thermal desorption spectroscopy (TDS) and high-resolution electron energy loss spectroscopy (HREELS). In this section we will focus on the formation of physisorbed and chemisorbed states of oxygen on Ag(110) and some of their NIR properties. A detailed discussion of the lifetime and energy of the O_2^- ($^4\Sigma_u^-$) resonance in the case of physisorbed O_2 on Ag(110) is shown in section 4.1, while the corresponding analysis of the angular distribution of the electron inelastically scattered is presented in section 4.2. The experimental details of the present section can be found in [104] and [105].

Figures 18(a) and (b) show TD spectra for oxygen adsorbed on Ag(110) at 15 K (18(a)) and 75 K (18b), respectively. First, TD measurements were made from a range of O_2 coverages initially deposited at 15 K. TD spectra, figure 18(a), were recorded using mass 32 signal, corresponding to molecular O_2. The main desorption peaks were observed at 59 and 100 K for low exposures (0.05–3 L) with extra peaks appearing at progressively higher exposures (3–10 L), first at 38 K and then at 36 K. These later peaks can be associated with the desorption

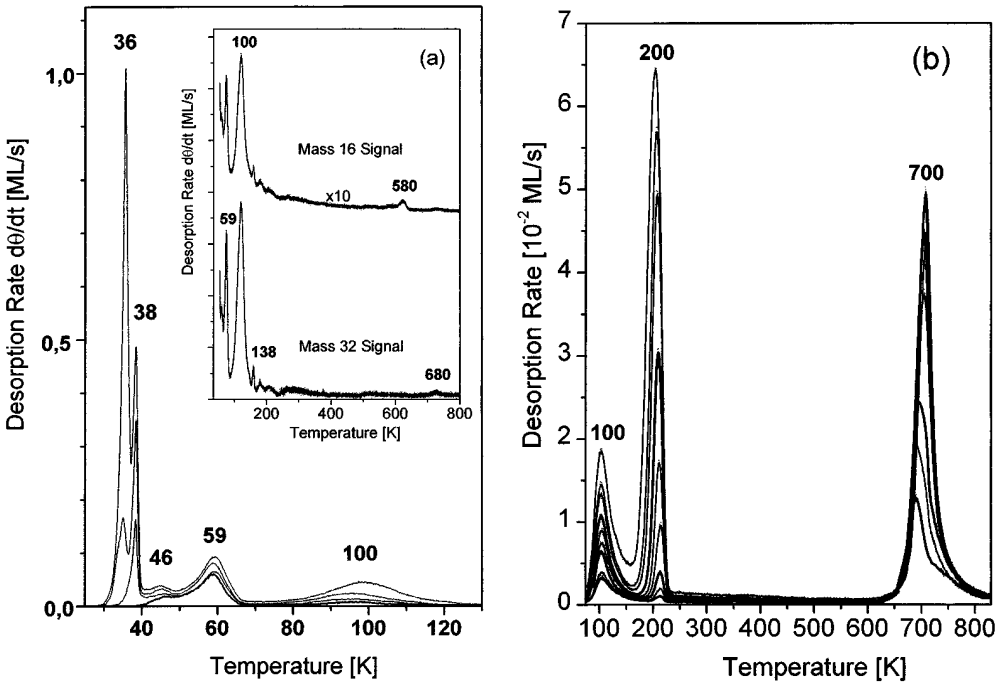

Figure 18. (a) TD spectra after the adsorption of oxygen on Ag(110) at 15 K for exposures from 0.1 to 10 L. The inset shows the TD spectra (at a temperature range from 40 to 800 K) after the exposure of 25 L O_2. (b) A set of TD spectra after the adsorption of O_2 on Ag(110) at 75 K for exposures from 50 to 2000 L. In both cases the spectra were taken for temperatures up to 830 K with a heating rate of 0.5 K s^{-1}.

of the physisorbed multilayer (36 K) and the second physisorbed layer (38 K). The desorption of the first physisorbed layer occurs at 59 K while the peak at 100 K is attributed to the chemisorbed molecular species which we shall denote α-O_2. From a detailed analysis of the relative intensities of the TD peaks we can estimate that a roughly constant proportion, about 20%, of the physisorbed O_2 converts into the chemisorbed species, α-O_2, upon warming. No significant desorption was observed for temperatures higher than 100 K. The oxygen molecules are only adsorbed in chemisorbed and physisorbed molecular states.

The TDS peak of the monolayer saturated only after adsorption of $\approx$20 L, while at this exposure already desorption from the second layer and from the multilayers are observed. In a detailed analysis Bartolucci [37] showed that the growing mechanism of oxygen on Ag(110) at 15 K is in islands. Therefore, the second layer starts to grow at 2.5 L of O_2, while only 35% of the monolayer is occupied. Desorption from multilayers is observed at 10 L, where 60% of the monolayer is occupied. The TDS peak at 100 K is attributed to oxygen chemisorbed on Ag(110). In this circumstances it is notable that no significant TDS peak is found at higher temperature. This is clearly shown in the inset showing TD spectra which were taken for 25 L O_2. Only a very low (negligible) peak around 680 K is shown for mass 32 which is not related to the peak at 580 K found for mass 16. This shows that no dissociative adsorption occurs after adsorption of oxygen at 15 K.

Thermal desorption measurements were also made from O_2 layers adsorbed at 75 K (figure 18(b)). Because of the vastly lower sticking probability at this temperature [21] the TD spectra were taken for an exposure range from 50 to 2000 L. At all exposures three desorption

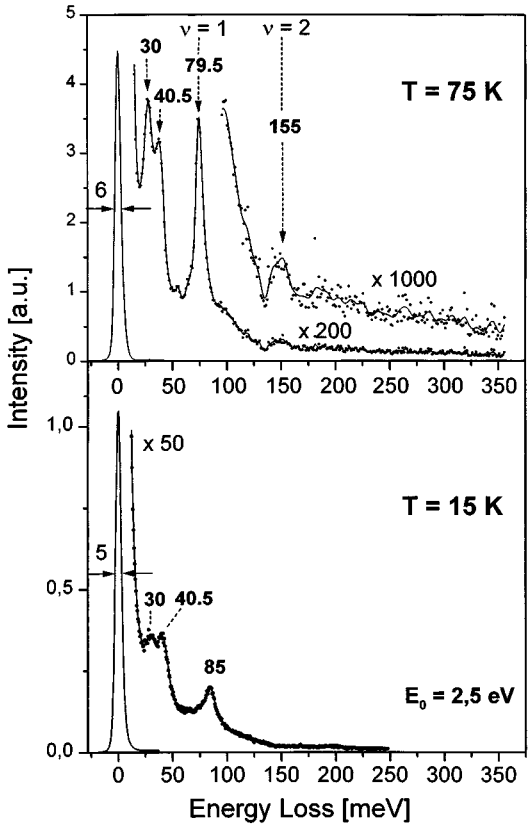

Figure 19. HREEL spectra of oxygen adsorbed on Ag(110) at 15 K (bottom) and 75 K (top), respectively.

peaks at around 100, 200 and 700 K were observed. The peak at ≈100 K again originates from desorption of α-O_2. The desorption peaks observed at ≈200 K and ≈700 K compare with previous reported values [5, 8] in the range 150–180 K for molecularly chemisorbed O_2 and 580–620 K for atomic O, thus we attribute the peak at ≈200 K to the well known chemisorbed species produced by dosing at ≈110 K (which we now denote β-O_2), while the peak seen at 700 K is due to the recombinative desorption of atomic oxygen. The slightly higher desorption temperatures are probably due to our calibration, which is optimised for the range <100 K. The features of figure 18(b) should be compared with the minimal desorption observed at higher temperatures (⩾120 K) from the layer prepared at 15 K (see inset of figure 18(a)). The comparison highlights two key points. First, the β-O_2 species is not produced by warming the physisorbed layer (no peak at 200 K in figure 18(a)). Second, α-O_2 does not dissociate to atomic O (no desorption at 700 K in figure 18(a)). This implies that α-O_2 does not convert to β-O_2 upon warming. This suggests that only α-O_2 is formed from the conversion of the physisorbed precursor and only β-O_2 dissociates to atomic O.

Figure 19 (spectrum at the bottom) shows an HREEL spectrum of 5 L O_2 on Ag(110) recorded in the specular direction at a primary energy of 2.5 eV. It exhibits three losses at 30, 40.5 and 85 meV. The loss at 30 meV is attributed to the O_2–Ag stretching vibration. This assignment is in accordance with the stretching vibration of oxygen chemisorbed on different surfaces [6, 8, 106]. The loss at 40.5 meV cannot be attributed univocally: on the one hand

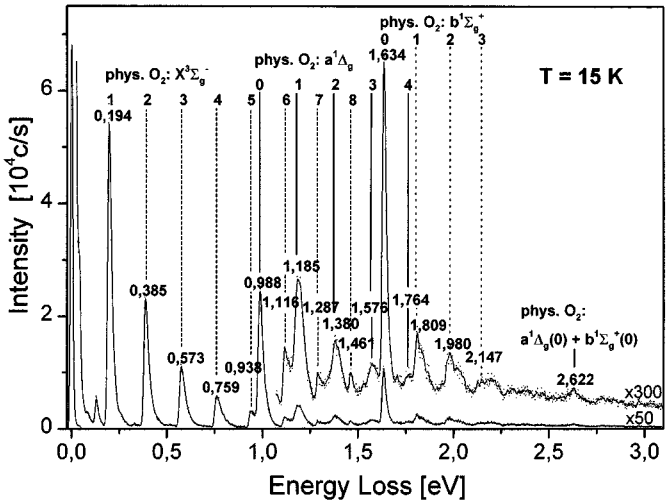

Figure 20. HREEL spectrum recorded for a wide-range scan of 3.0 eV for 20 L of oxygen adsorbed on Ag(110) at 15 K.

the frequency corresponds to the vibrations of atomic oxygen against the Ag(110) surface [6, 13], and on the other hand for oxygen adsorption at 15 K no evidence for a dissociative adsorption was found in our TDS investigations. The loss at 85 meV is assigned to the stretching vibration of chemisorbed molecules of oxygen in the α-O_2 state. The spectrum at the top of figure 19 was recorded after adsorption of 1000 L of O_2 at 75 K. The frequency of the stretching vibration of chemisorbed oxygen is now found at 79.5 meV showing that the molecules are adsorbed in a different state which has already been denoted by β-O_2. These findings are in accordance with the TDS data presented above and discussed in a previous paper [38].

Figure 20 shows an HREEL spectrum of 20 L O_2 adsorbed on Ag(110) at 15 K. The HREEL spectrum was recorded in an energy range of 3 eV at an energy resolution of 9 meV. The primary electron energy was fixed at 9.3 eV and a scan step width of 2.5 meV was chosen in order to gain intensity. In this spectrum several electronical and vibrational excitations can be observed. In the low-energy region losses at 85 and 194 meV are observed. The loss at 85 meV corresponds to the stretching vibration of oxygen chemisorbed in the α-state. The loss at 194 meV is attributed to the stretching vibration of O_2 molecule physisorbed on the surface in the neutral ground state $X^3\,\Sigma_g^-$. In the gas phase the stretching vibration for oxygen has a value of 194 meV [72]. Therefore, the assignment of the loss at 194 meV is univocal. For the mode at 194 meV overtone excitations at 0.385, 0.573, 0.759, 0.938, 1.116, 1.287 and 1.461 eV are observed. The line-shape of the loss at 194 meV and the related overtones show an asymmetry with a tail on the high-energy site. This asymmetry lineshape is a quite general feature, observed for adsorbed O_2 on other Ag surfaces and for other systems (see section 3). The transition from the ground state to the first electronical excited state $a^1\,\Delta_g$ is observed at 0.988 eV together with the corresponding fundamental vibrational excitation at 1.185 eV and its overtones at 1.380, 1.576 and 1.764 eV. The excitation of the $b^1\,\Sigma_g^+$ state is seen at 1.634 eV. In addition, the fundamental of the stretching mode and the corresponding overtones at 1.809, 1.980 and 2.147 eV are observed. The loss at 2.622 eV corresponds to a combination loss of the excitation of the states $a^1\,\Delta_g(0)$ and $b^1\,\Sigma_g^+(0)$, respectively. The zeros in the parentheses represent the vibrational ground state.

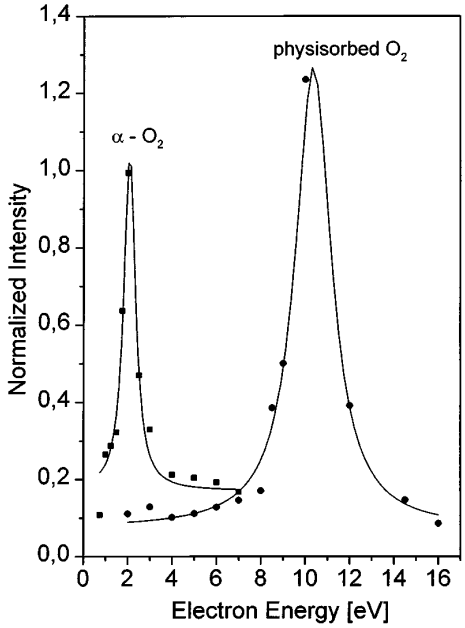

Figure 21. Resonance curves of oxygen chemisorbed in the α-state (mode at 85 meV) and physisorbed (mode at 194 meV) on Ag(110) at 15 K.

Figure 21 shows the normalized intensity of the loss at 85 and 194 meV, respectively, versus the primary energy of the electrons. The resonance curve for chemisorbed O_2 (mode at 85 meV) was measured for an exposure of 5 L, while that for the loss at 194 meV (physisorbed O_2) was measured after an exposure of 20 L. Both the adsorption and the HREELS measurement were performed at 15 K. The exposure of 20 L oxygen corresponds to an oxygen film of approximately seven monolayers. For the mode at 85 meV a sharp maximum was found at 2.0 eV. The FWHM (full width at half maximum) is approximately 1.5 eV. A similar resonance effect was found for oxygen chemisorbed on Pd(111) [107]. In that case the resonance curves show a maximum at 1–1.5 eV and the frequency of the stretching vibration lies at 104 meV. For the physisorbed molecules, corresponding to the loss at 194 meV the maximum is located at $\approx$10 eV with an FWHM of 2.5 eV. In recent studies of O_2/Ag(110) the maximum of the resonance curve was found at around 9 eV and was attributed to the excitation of the $^4\Sigma_u^-$ resonance [67, 89].

In conclusion, the TDS and HREELS measurements show that the oxygen is chemisorbed on Ag(110) in two different states. The α-state is characterized by a desorption temperature centred at 100 K and the frequency of the stretching vibration of the O_2 molecules lies at 85 meV. The β-state has a desorption temperature centred at 200 K and the frequency of the stretching vibration has a value of 79.5 meV. The α-state occurs in coexistence with physisorbed oxygen and can also be prepared by conversion of physisorbed oxygen. The intensity of the loss corresponding to the stretching vibration of oxygen has a maximum at around 2 eV, which is a characteristic of the formation of a short-lived negative ion. The β-state does not show resonance effects. For the multilayer regime of O_2 physisorbed on Ag(110) a maximum in the resonance curve is found at 10 eV showing an excitation of the $^4\Sigma_u^-$ resonance. The α-state does not dissociate to atomic O.

6. Summary

The adsorption of O_2 on the (100), (110) and (111) surfaces of silver has been investigated with a number of complementary techniques. The thermodynamic aspects of the adsorption of oxygen on silver were studied by measuring the sticking coefficient and by TDS. A comparison between the adsorption properties of O_2 on different crystallographic silver surfaces (Ag(100), Ag(110) and Ag(111)) has been presented. In summary, we have shown via supersonic molecular beam studies that the O_2–Ag interaction is strongly face dependent and characterized by the dependence of the sticking coefficient on energy and angle of incidence of the gas-phase molecules. The HREELS investigation showed the presence of two major molecular species for both the (110) and the (001) faces. For Ag(110) one moiety desorbs upon heating the crystal to 100 K, while the other leads to dissociation above 150 K. For Ag(001), in contrast, both dioxygen moieties lead to desorption. Only a minority species, associated with the very low internal stretching frequency of 64 meV, undergoes dissociation on heating.

The Ag(111) surface is very suitable for the study of physisorption of O_2 since the competing channel of non-dissociative chemisorption is very unlikely; we found the initial sticking coefficient for non-dissociative chemisorption to be smaller than 10^{-8}. For physisorbed O_2 the intramolecular stretching mode at 192 meV (monolayer) exhibits strong overtones and inelastic tails due to combination losses, both typical of NIR formation. The same behaviour is observed for multilayers. The vibrational features typical of NIR are very similar to those found for physisorbed N_2, another homonuclear molecule.

Oxygen is molecularly chemisorbed on Ag(110) in two different states. The α-state coexists with physisorbed oxygen, and is characterized by a desorption temperature centred at 100 K and a vibrational stretching vibration of 85 meV. This vibrational mode also shows NIR properties with a resonance energy at around 2 eV. The β-state desorbs at 200 K and the molecular stretching frequency has a value of 79.5 meV. No resonance was observed in this case.

A simple model was developed for the angular properties of a resonantly scattered electron. This model links the electron angular distribution to the symmetry of the NIR intermediate and to the orientation with respect to the surface of the molecular axis of an isolated physisorbed molecule. It also takes into account the effect of refraction due to the electron–metal interaction on the electron scattering. This model allows a quantitative interpretation of the measurements of the polar angle distributions for physisorbed O_2 on Ag(110). The molecular axis orientation so obtained, and its dependence upon coverage, is in agreement with a previous determination based on NEXAFS measurements. Furthermore, the model study shows that ambiguities in the determination of the molecular axis orientation could be removed if the theoretical analysis were based on a complete measurement of the angular distribution, both in azimuth and polar angles.

Acknowledgment

This work was supported by the EU (HCM programme contract ERB CHRXCT930326).

References

[1] Besenbacher F and Norskov J K 1993 *Prog. Surf. Sci.* **44** 5
[2] Campbell C T and Paffett M 1984 *Surf. Sci.* **139** 396
Van Santen R A and Kuipers H P C 1990 *Adv. Catal.* **35** 256
[3] Engelhardt H A and Menzel D 1976 *Surf. Sci.* **57** 591

[4] Campbell C T 1985 *Surf. Sci.* **157** 43
Campbell C T 1986 *Surf. Sci.* **173** L641
[5] Barteau M A and Madix R J 1980 *Surf. Sci.* **97** 101
[6] Sexton B A and Madix R J 1980 *Chem. Phys. Lett.* **76** 294
[7] Bowker M 1980 *Surf. Sci.* **100** L472
[8] Backx C, De Groot C P M and Biloen P 1981 *Surf. Sci.* **104** 300
[9] Bange K, Madey T E and Sass J K 1985 *Chem. Phys. Lett.* **113** 56
[10] Prince K C, Paolucci G and Bradshow A M 1986 *Surf. Sci.* **175** 101
[11] Stoehr J and Outka D A 1987 *Phys. Rev.* B **36** 7891
[12] Upton T H, Stevens P and Madix R J 1988 *J. Chem. Phys.* **88** 3988
[13] Tjeng L H, Meinders M B and Sawatzky G A 1990 *Surf. Sci.* **223** 341
[14] Puschmann A and Haase J 1984 *Surf. Sci.* **144** 559
Becker L, Aminpirooz S, Schmalz A, Hillert B, Pedio M and Hasse J 1991 *Phys. Rev.* B **44** 13 655
[15] Bracco G, Tatarek R and Vandoni G 1990 *Phys. Rev.* B **42** 1852
[16] Guest R J, Hernnäs B, Bennich P, Bjørneholm O, Nilsson A, Palmer R E and Märtensson N 1992 *Surf. Sci.* **278** 239
[17] Taniguchi M, Tanaka K, Hashizume T and Sakurai T 1992 *Surf. Sci.* **262** L123
Hashizume T 1992 *Surf. Sci.* **266** 282
[18] Rocca M, Vattuone L, Boragno C and Valbusa U 1993 *J. Electron Spectrosc. Relat. Phenom.* **64/65** 577
[19] Vattuone L, Boragno C, Pupo M, Restelli P, Rocca M and Valbusa U 1994 *Phys. Rev. Lett.* **72** 510; the data taken from this paper, and reported in figure 4, were corrected for the error in the energy calibration.
[20] Vattuone L, Rocca M, Restelli P, Pupo M, Boragno C and Valbusa U 1994 *Phys. Rev.* B **49** 5113
[21] Vattuone L, Rocca M, Boragno C and Valbusa U 1994 *J. Chem. Phys.* **101** 713; the data taken from this paper, and reported in figure 4, were corrected for the error in the energy calibration. See also Rocca M 1996 *Phys. Scr.* T **66** 262
[22] Vattuone L, Rocca M, Boragno C and Valbusa U 1994 *J. Chem. Phys.* **101** 726
[23] Pai W W, Bartelt N C, Peng M R and Reutt-Robey J E 1995 *Surf. Sci.* **330** L679
[24] Canepa M, Cantini P, Mattera L, Terreni S and Valdenazzi F 1992 *Phys. Scr.* T **41** 226
Canepa M, Salvietti M, Traverso M and Mattera L 1995 *Surf. Sci.* **331–333** 183
[25] Spruit M E M and Kleyn A W 1989 *Chem. Phys. Lett.* **159** 342
[26] Raukema A and Kleyn A W 1995 *Phys. Rev. Lett.* **74** 4333
[27] Buatier de Mongeot F, Valbusa U and Rocca M 1995 *Surf. Sci.* **339** 291
[28] Garfunkel E L, Ding X, Dong G, Yang S, Hou X and Wang X 1985 *Surf. Sci.* **164** 511
[29] Ares Fang C S 1990 *Surf. Sci.* **235** L291
[30] Rocca M, Traversaro P and Valbusa U 1990 *J. Electron Spectrosc. Relat. Phenom.* **54/55** 131
[31] Torras J, Ricart J M, Illas F and Rubio J 1993 *Surf. Sci.* **297** 57
[32] Buatier de Mongeot F, Valbusa U and Rocca M 1996 *Surf. Sci.* **363** 68
[33] Van der Hock P J and Baerends E J 1989 *Surf. Sci.* **221** 1791
[34] Buatier de Mongeot F, Cupolillo A, Valbusa U and Rocca M 1997 *Chem. Phys. Lett.* **270** 345
[35] Rocca M 1996 *Phys. Scr.* T **66** 202
[36] Lacombe S, Cemic F, He P, Dietrich R, Geng P, Rocca M and Jacobi K 1996 *Surf. Sci.* **368** 38
[37] Bartollucci F 1997 *PhD Thesis* Heinrich-Heine-Universität Düsseldorf
[38] Bartollucci F, Franchy R, Barnard J C and Palmer R E 1998 *Phys. Rev. Lett.* **80** 5224
[39] Vattuone L, Gambardella P, Rocca M and Valbusa U 1997 *Surf. Sci.* **377/379** 671
[40] Sanche L 1990 *J. Phys. B: At. Mol. Opt. Phys.* **23** 1597
[41] Palmer R E and Rous P J 1992 *Rev. Mod. Phys.* **64** 383
[42] Schulz G L 1973 *Rev. Mod. Phys.* **45** 423
[43] Andersson S and Davenport J W 1978 *Solid State Commun.* **28** 677
[44] Sanche L and Michaud M 1984 *J. Chem. Phys.* **81** 257
[45] Demuth J E, Schmeisser D and Avouris Ph 1981 *Phys. Rev. Lett.* **47** 1166
[46] Raukema A, Butler D A, Box F M A and Kleyn A 1996 *Surf. Sci.* **347** 151
[47] Jones T S and Richardson N V 1988 *Phys. Rev. Lett.* **61** 1752
[48] Jacobi K, Bertolo M and Hansen W 1990 *J. Electron. Spectrosc. Relat. Phenom.* **54/55** 529
[49] Scoles G, Laine M and Valbusa U (eds) 1992 *Molecular Beam Methods* (Oxford: Oxford University Press)
[50] Rocca M, Valbusa W, Gussoni A, Maloberti G and Racca L 1991 *Rev. Sci. Instrum.* **62** 2172
[51] King D A and Wells M G 1972 *Surf. Sci.* **29** 454
Vattuone L, Burghaus U, Valbusa U and Rocca M 1998 *Surf. Sci.* **408** L693
[52] Kleyn A, Butler D A and Raukema A 1996 *Surf. Sci.* **363** 29

[53] Luntz A C, Williams M D and Bethune D S 1988 *J. Chem. Phys.* **89** 4381
Rettner C T and Mullins C B 1991 *J. Chem. Phys.* **94** 1626
[54] Rettner C T, Schweizer E K and Stein H 1990 *J. Chem. Phys.* **93** 1442
[55] Rettner C T and Stein H 1988 *Phys. Rev. Lett.* **59** 2768
[56] Darling G R and Holloway S 1994 *Surf. Sci.* **321** L189
[57] Carley A F, Davies P R, Roberts M W and Thomas K K 1990 *Surf. Sci.* **238** L467
[58] Buatier de Mongeot F, Cupolillo A, Rocca M, Valbusa U, Kreuzer J and Payne S H 1997 *J. Chem. Phys.* **107** 711
[59] Buatier de Mongeot F, Cupolillo A, Rocca M and Valbusa U 1997 *J. Chem. Phys.* **106** 9296
[60] Akerlund C, Zoric I, Kasemo B, Cupolillo A, Buatier de Mongeot F and Rocca M 1997 *Chem. Phys. Lett.* **270** 157
[61] Vattuone L, Gambardella P, Cemic F, Valbusa U and Rocca M 1997 *Chem. Phys. Lett.* **278** 245
Valuone L, Gambordella P, Burghaus U, Cemic F, Cupolillo A, Valbusa V and Rocca M 1998 *J. Chem. Phys.* **109** 2490
[62] Rocca M, Cemic F, Buatier de Mongeot F, Valbusa U, Lacombe S and Jacobi K 1997 *Surf. Sci.* **373** 125
[63] Butler D A, Reukema A and Kleyn A W 1969 *J. Chem. Soc. Faraday Trans.* **92** 2319
[64] Jacobi K, Astaldi C, Geng P and Bertolo M 1989 *Surf. Sci.* **223** 569
[65] Schmeisser D, Demuth J E and Avouris P 1982 *Phys. Rev.* B **26** 4857
[66] Wong S F, Boness M J W and Schultz G J 1973 *Phys. Rev. Lett.* **31** 969
[67] Tang K B K, Rous P J and Palmer R E 1995 *Phys. Rev.* B **52** 12 395
[68] Hansen W 1991 *Dissertation* TU Berlin
[69] Jacobi K and Bertolo M 1990 *Phys. Rev.* B **42** 3733
[70] Guyters M and Jacobi K 1994 *Chem. Phys. Lett.* **225** 309
[71] Tang K B K, Villette J, Teillet-Billy D, Gauyacq J P and Palmer R E 1996 *Surf. Sci.* **368** 43
[72] Herzberg G 1950 *Spectra of Diatomic Molecules* (New York: Van Nostrand-Reinhold)
[73] Hansen W, Bertolo M and Jacobi K 1991 *Surf. Sci.* **253** 1
[74] Lacombe S, Cemic F, Jacobi K, Hedhili M N, LeCoat Y, Azria R and Tronc M 1997 *Phys. Rev. Lett.* **79** 1146
[75] Allan M, Asmis K R, Propovic D B, Stepanovic M, Mason N J and Davies J A 1996 *J. Phys. B: At. Mol. Opt. Phys.* **29** 4727
[76] Jensen E T, Palmer R E and Rous P J 1990 *Phys. Rev. Lett.* **64** 1301
[77] Rous P J, Jensen E T and Palmer R E 1989 *Phys. Rev. Lett.* **63** 2496
[78] Gadzuk J W 1983 *J. Chem. Phys.* **79** 3982
[79] Gadzuk J W 1988 *Annu. Rev. Phys. Chem.* **39** 395
[80] Rous P J 1995 *Phys. Rev. Lett.* **74** 1835
[81] Rous P J 1996 *Phys. Rev.* B **53** 11 076.
[82] Rous P J 1995 *Surf. Sci.* **326** 67
[83] Rous P J and Hartley D M 1995 *Chem. Phys. Lett.* **236** 299
[84] Rous P J 1992 *Surf. Sci. Lett.* **279** L191
[85] Šiller L, Wendelken J F, Hock K M and Palmer R E 1993 *Chem. Phys. Lett.* **210** 15
[86] Gerber A and Herzenberg A 1985 *Phys. Rev.* B **31** 6219
[87] Teillet-Billy D, Djamo V and Gauyacq J P 1992 *Surf. Sci.* **270** 425
[88] Djamo V, Teillet-Billy D and Gauyacq J P 1995 *Phys. Rev.* B **51** 5418
[89] Tang K B K and Palmer R E 1996 *Phys. Rev.* B **53** 1099
[90] Azria R, Parenteau L and Sanche L 1987 *Phys. Rev. Lett.* **59** 638
[91] Silva L A and Palmer R E 1992 *Surf. Sci.* **272** 313
[92] Azria R, Coat Y L, Mharzi B and Tronc M 1995 *Nucl. Instrum. Methods* B **101** 184
[93] Sambe H and Ramaker D E 1989 *Phys. Rev.* A **40** 3651
[94] Sambe H, Ramaker D E, Deschenes M, Bass A D and Sanche L 1990 *Phys. Rev. Lett.* **64** 523
[95] Andrick D and Read F H 1971 *J. Phys. B: At. Mol. Phys.* **4** 389
Andrick D and Read F H 1971 *J. Phys. B: At. Mol. Phys.* **4** 911
[96] Davenport J W, Ho W and Schrieffer J R 1978 *Phys. Rev.* B **17** 3115
[97] Barnard J C and Palmer R E 1992 *Surf. Sci.* **269/270** 420
[98] Jensen E T, Palmer R E and Rous P J 1990 *Phys. Rev. Lett.* **64** 1301
[99] Rous P J, Palmer R E and Willis R F 1989 *Phys. Rev.* B **39** 7552
[100] Palmer R E, Rous P J, Wilkes J K and Willis R F 1988 *Phys. Rev. Lett.* **60** 329
[101] Allan M 1995 *J. Phys. B: At. Mol. Opt. Phys.* **28** 5163
[102] Teillet-Billy D and Gauyacq J P 1991 *Nucl. Instrum. Methods* B **58** 393
Teillet-Billy D and Gauyacq J P 1995 *Nucl. Instrum. Methods* B **101** 88

[103] Guest R J, Hernnäs B, Bennich P, Björneholm O, Nilsson A, Palmer R E and Mårtensson N 1992 *Surf. Sci.* **278** 239
[104] Bartolucci F and Franchy R 1996 *Surf. Sci.* **368** 27
[105] Bartolucci F, Franchy R, Silva J A M C, Moutinho A M C, Teillet-Billy D and Gauyacq J P 1998 *J. Chem. Phys.* **108** 2251
[106] Vattuone L, Rocca M and Valbusa V 1994 *Surf. Sci.* **314** 904
[107] Cemic F, Dippel O, Kolasinski K W and Hasselbrink E 1995 *Surf. Sci.* **331–333** 267